

# Prebiotic Environmental Conditions Impact the Type of Iron-Sulfur Cluster Formed

Luca Valer,<sup>[a]</sup> Yin Juan Hu,<sup>[b]</sup> Alberto Cini,<sup>[c]</sup> Marco Lantieri,<sup>[c]</sup> Craig R. Walton,<sup>[d]</sup> Oliver Shorttle,<sup>[d]</sup> Maria Fittipaldi,<sup>[c]</sup> and Sheref S. Mansy<sup>\*[a, b]</sup>

Iron-sulfur clusters are ancient cofactors that could have played a role in the prebiotic chemistry leading to the emergence of protometabolism. Previous research has shown that certain iron-sulfur clusters can form from prebiotically plausible components, such as cysteine-containing oligopeptides. However, it is unclear if these iron-sulfur clusters could have survived in prebiotically plausible environments. To begin exploring this possibility, we tested the stability of iron-sulfur clusters coordinated to a tripeptide and to *N*-acetyl-L-cysteine

methyl ester in a variety of solutions meant to mimic prebiotically plausible environments. We also assessed the impact of individual chemical components on stability. We find that iron-sulfur clusters form over a wide variety of conditions but that the type of iron-sulfur cluster formed is strongly impacted by the chemical environment and the coordinating scaffold. These findings support the general hypothesis that iron-sulfur clusters were present on the prebiotic Earth and that different types of iron-sulfur cluster predominated in different environments.

## Introduction

Iron-sulfur clusters are widely believed to be ancient cofactors that may have participated in the prebiotic chemistry that led to the first cells on Earth.<sup>[1]</sup> Although much is known regarding the synthesis of iron-sulfur clusters in organic solvent, it is only recently that analogous synthesis in aqueous solution has become more common.<sup>[2]</sup> Small organic thiolates and small ( $\leq 3$  aa) cysteine-containing peptides, including glutathione (E $\gamma$ CG), can coordinate to mononuclear iron ions and [2Fe–2S] and [4Fe–4S] clusters in water.<sup>[3]</sup> Additionally, hexa- and dodeca-peptide sequences representing fusion products of a tripeptide suggest that iron-sulfur cluster templated peptide-bond formation could have led to the prebiotic generation of modern day iron-sulfur motifs.<sup>[4]</sup> However, there are no examples of attempts to synthesize iron-sulfur clusters under reasonable prebiotic environmental conditions. To gain some insight into whether iron-sulfur peptides could have survived the environmental conditions of the early Earth, we selected four different model prebiotic conditions, including alkaline lakes,<sup>[5]</sup> alkaline hydrothermal vents (lost city),<sup>[6,7]</sup> prebiotic

seawater,<sup>[8]</sup> and glacial brine<sup>[9]</sup> conditions (Table S1). We evaluated if iron-sulfur clusters formed at each of these conditions and, if so, if the environment affected which type of iron-sulfur cluster predominated.

We used an interference chemistry approach to test the environmental sensitivity of iron-sulfur clusters, i.e., we subjected our prebiotic species of interest to complex and environmentally realistic solution compositions.<sup>[10]</sup> The solution compositions were chosen to span a wide range of prebiotically plausible environments from subaerial ponds to dilute ocean water and hydrothermal systems. Altogether, these conditions spanned the majority of environments usually considered in the study of life's origins.

Whilst the complex solutions applied in interference chemistry may be generally informative about whether iron-sulfur clusters may have formed in alkaline lakes, for example, this approach lacks specificity. Many variants of a given prebiotic environment may exist, so it is important to attempt to isolate which interferences are most problematic for iron-sulfur cluster stability. For this reason, we also conducted variable concentration studies of individual interfering chemical species (Table S2–S3). The formation of iron-sulfur clusters was assessed by a combination of UV-Vis absorption and Mössbauer spectroscopies. The organic thiols used to stabilize the formation of the iron-sulfur cluster were *N*-acetyl-L-cysteine methyl ester (NAC-Cys-OMe) and E $\gamma$ CG.

## Results and Discussion

### Prebiotic Environments Affect the Formation of Iron-Sulfur Clusters

To determine if iron-sulfur clusters could have formed under prebiotic conditions we added 10 mM organic thiol (NAC-Cys-OMe or E $\gamma$ CG), 2.5 mM FeCl<sub>3</sub>, and 2.5 mM Na<sub>2</sub>S to each


[a] D-CIBIO, University of Trento, Trento, Italy


[b] Department of Chemistry, University of Alberta, Edmonton, Alberta, Canada

[c] INSTM and Department of Physics and Astronomy, University of Florence, Sesto Fiorentino (FI), Italy

[d] Department of Earth Sciences, University of Cambridge, Cambridge, Cambridgeshire, United Kingdom

**Correspondence:** Sheref S. Mansy, D-CIBIO, University of Trento, via Sommarive 9, 38123 Trento, Italy.  
Email: [sheref.mansy@ualberta.ca](mailto:sheref.mansy@ualberta.ca)

 Supporting Information for this article is available on the WWW under <https://doi.org/10.1002/syst.202400051>

 © 2024 The Author(s). ChemSystemsChem published by Wiley-VCH GmbH. This is an open access article under the terms of the Creative Commons Attribution Non-Commercial License, which permits use, distribution and reproduction in any medium, provided the original work is properly cited and is not used for commercial purposes.

anaerobic environmental condition. This was necessary so that we had enough iron-sulfur cluster to measure. In other words, we did not probe the impact of environmental concentrations of iron and sulfide ions but instead assumed that the components necessary to form an iron-sulfur cluster were present. However, both lost city and seawater likely would have had, the former also in the present day, appreciable levels of dissolved iron and sulfide; alkaline lake and glacial brine plausibly also contained iron, while the sulfide might have been provided in reduced form from the underlying sediment. For all the conditions tested, UV-Visible absorption spectra were acquired and were analyzed by spectral decomposition with Fit-FeS<sup>[11]</sup> using reference spectra (Figure S1–S2) for a mononuclear centre in addition to [2Fe–2S] and [4Fe–4S] clusters. Subsequently, the samples were then precipitated and analyzed by Mössbauer spectroscopy at 80 K (Figure 1B–D, Figure S3, Table S4–S5). All spectra appeared as the overlap of multiple

contributions having the shape of doublets, as expected.<sup>[3]</sup> Moreover, the fit of the spectra revealed the hyperfine interactions of the <sup>57</sup>Fe ions of each sample, which were used to identify the oxidation state of iron and the type of iron-sulfur clusters present. The contributions of the Mössbauer spectra were used to calculate the percentage of the cluster types in each sample (Table S6). The coefficients of determination ( $r^2$ ) between the fits of UV-vis and Mössbauer data sets were 0.75, 0.68, and 0.89 for mononuclear centres, [2Fe–2S] clusters, and [4Fe–4S] clusters, respectively (Figure 1E–G). Therefore, the fitting of UV-Vis data (Figure S4–S11, Table S7) gave a semi-quantitative indication of the iron-sulfur composition at each condition and was used for the remaining analyses.

NAC-Cys-OME and E<sub>γ</sub>CG were affected similarly by the tested environmental conditions for the stability of polynuclear iron-sulfur clusters. There was no correlation for the amount of mononuclear centre ( $\rho=0.04$ ) between the data with NAC-Cys-

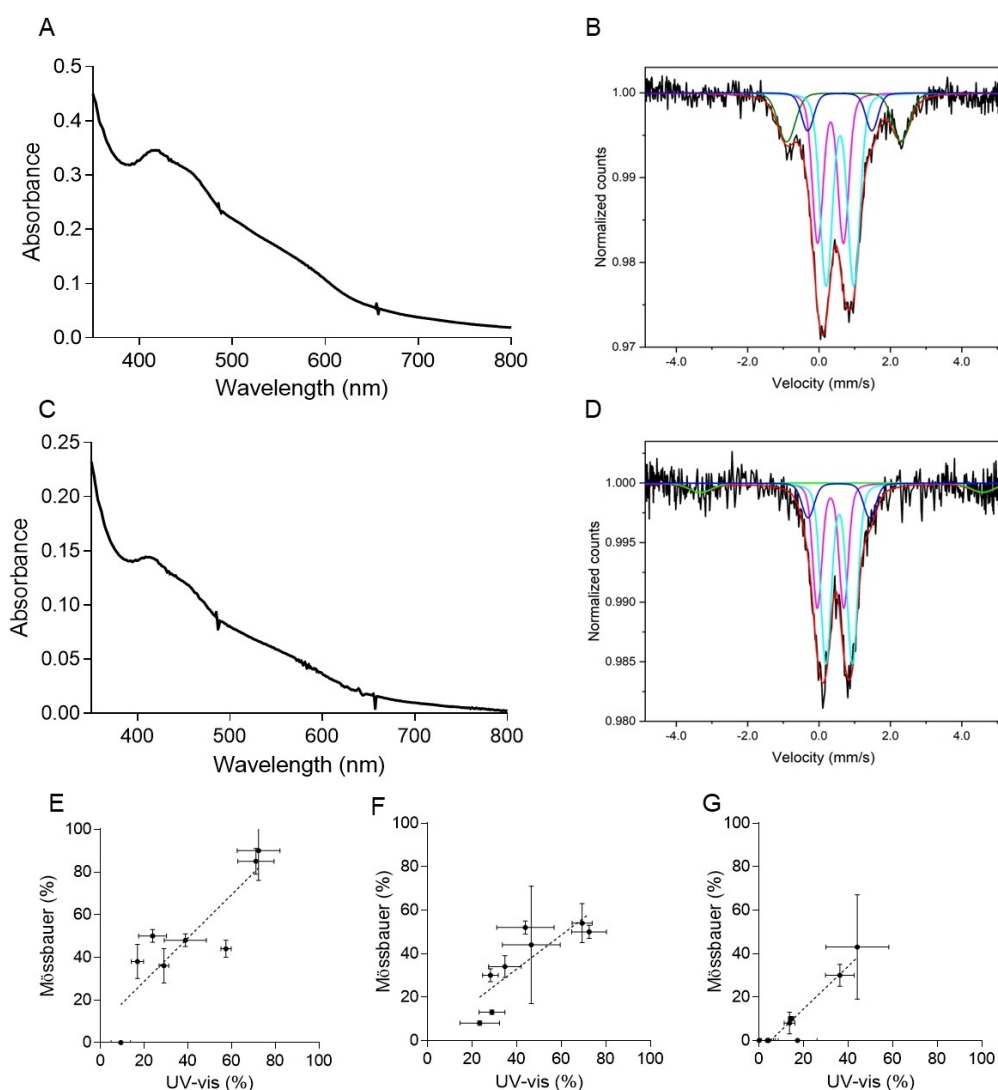


**Figure 1.** UV-vis and Mössbauer spectra of iron-sulfur clusters in solutions meant to mimic the environment of the Lost City. UV-Vis (A, C) and Mössbauer (B, D) spectra acquired at 80 K of E<sub>γ</sub>CG (A, B) and NAC-Cys-OME (C, D). In B and D, the fit (red line) and the contributions of each type of iron-sulfur cluster (coloured lines) are also reported (see SI for details). E, F, G) Correlation plots of Mössbauer and UV-vis data for NAC-Cys-OME and E<sub>γ</sub>CG acquired in the four tested prebiotic conditions. Plots are of correlations for mononuclear centre (E, slope:  $1.01 \pm 0.23$ ), [2Fe–2S] cluster (F, slope:  $0.78 \pm 0.21$ ), and [4Fe–4S] cluster (G, slope:  $0.97 \pm 0.13$ ).

OMe and E $\gamma$ CG (Figure S12). However, the amount of [2Fe–2S] ( $\rho=0.76$ ) and [4Fe–4S] ( $\rho=0.87$ ) cluster formed on NAc-Cys-OMe and E $\gamma$ CG showed some degree of correlation (Figure S14). The data indicated that the environmental conditions strongly impacted the type of iron-sulfur cluster formed in a way that was not devoid of the influences of the ligating organic molecule. For example, lost city conditions gave predominantly [4Fe–4S] cluster for E $\gamma$ CG. The same condition gave roughly equal amounts of [2Fe–2S] and [4Fe–4S] cluster for NAc-Cys-OMe (Figure 2). The impact of the environment was clear, with [2Fe–2S] clusters dominating when E $\gamma$ CG was placed in glacial brine conditions, whereas the other tested conditions either gave mostly mononuclear center (seawater and alkaline lake) or [4Fe–4S] cluster (Lost City) for E $\gamma$ CG.

### Iron-Sulfur Clusters are Sensitive to Individual Chemical Additives

To better define the impact of the environment on the stability of iron-sulfur clusters, we determined the iron-sulfur composition of E $\gamma$ CG and NAc-Cys-OMe in the presence of 100  $\mu$ M, 500  $\mu$ M, and 500 mM chemical additive by the decomposition of UV-vis spectra. For the majority of the 17 conditions tested, no strong effect was observed in the sense that mononuclear center, [2Fe–2S], and [4Fe–4S] clusters were detected in roughly the same ratios as the control condition in the absence of chemical additive (Figure 3, Table S8–S10). The exceptions included ferrous carbonate (FeCO<sub>3</sub>) and calcium carbonate

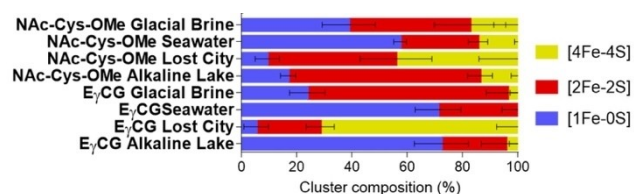


**Figure 2.** Iron-sulfur cluster composition of E $\gamma$ CG and NAc-Cys-OMe at different prebiotic conditions. Data are from the decomposition of UV-Vis absorption spectra (Table S7). Data represent mean and SD of distinct samples,  $n=3$ .

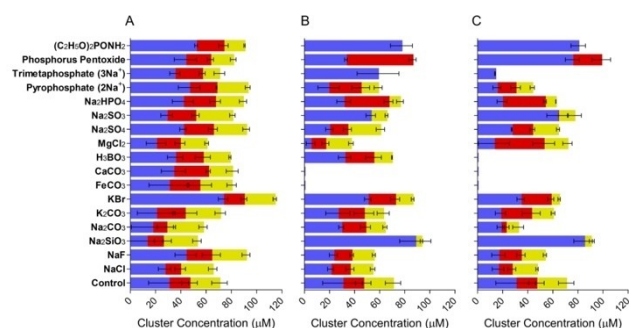


**Figure 3.** Iron-sulfur cluster composition of E $\gamma$ CG in the presence of different chemical additives at pH 8.7 and 100  $\mu$ M (A), 500  $\mu$ M (B), and 500 mM (C) chemical additive. Mononuclear center is in blue, [2Fe–2S] is in red, and [4Fe–4S] is shown in yellow. Data represent mean and SD of distinct samples,  $n=3$ .

(CaCO<sub>3</sub>) at 500  $\mu$ M and 500 mM, which completely removed the presence of all three types of iron-sulfur centers. These data were consistent with the substitution of Fe<sup>3+</sup> within the iron-sulfur cluster with either Fe<sup>2+</sup> or Ca<sup>2+</sup>. Biological iron-sulfur clusters typically require at least one Fe<sup>3+</sup> to be stable in aqueous solution.<sup>[12,13]</sup> The data were unlikely to have been influenced by carbonate, since K<sub>2</sub>CO<sub>3</sub> and Na<sub>2</sub>CO<sub>3</sub> did not destroy the iron-sulfur clusters even at 0.5 M. Boric acid (BH<sub>3</sub>O<sub>3</sub>) degraded the iron-sulfur cluster at 500 mM, consistent with the ability of borate to form a higher affinity complex with Fe<sup>3+</sup> than carbonate.

Diethyl phosphoramidate ((C<sub>2</sub>H<sub>5</sub>O)<sub>2</sub>PONH<sub>2</sub>) completely degraded the polynuclear iron-sulfur clusters at 500  $\mu$ M and above. We previously observed instability of iron-sulfur clusters with a nearby primary amine,<sup>[3]</sup> presumably due to competition between amino and thiolate groups for iron ions. Although phosphate (added as Na<sub>2</sub>HPO<sub>4</sub>) and pyrophosphate (added as Na<sub>2</sub>P<sub>2</sub>O<sub>7</sub>) did not significantly alter the distribution of iron-sulfur clusters, phosphorus pentoxide (P<sub>4</sub>O<sub>10</sub>) and trimetaphosphate (added as Na<sub>3</sub>P<sub>3</sub>O<sub>9</sub>) were more deleterious. Phosphorus pentoxide degraded the [4Fe–4S] cluster at 500  $\mu$ M and above, consistent with the mechanism of assembly of iron-sulfur clusters elucidated by Holm.<sup>[12]</sup> [4Fe–4S] clusters are built from two [2Fe–2S] clusters, and so the degradation of a [4Fe–4S] cluster may proceed through the formation of [2Fe–2S] clusters. The addition of trimetaphosphate had a stronger effect, leading to the loss of both [2Fe–2S] and [4Fe–4S] clusters. The reasons for the differing effects between these different phosphate containing molecules are unclear. It is reasonable to expect that each phosphate containing molecule has a different affinity for metals and has differing abilities to access the metal ions of the varied types of iron-sulfur clusters bound to organic thiolates. For example, each iron ion of a [2Fe–2S] cluster is bound by two peptidyl thiolates, whereas each iron ion of a [4Fe–4S] cluster is more exposed, bound by a single peptidyl thiolate.

The remaining chemical additives that disrupted the iron-sulfur clusters coordinated to E $\gamma$ CG were sodium metasilicate (Na<sub>2</sub>SiO<sub>3</sub>) and sodium sulfite (Na<sub>2</sub>SO<sub>3</sub>). Both negatively impacted polynuclear iron-sulfur clusters from 500  $\mu$ M and above. Iron-sulfur clusters were stable in the presence of sodium sulfate (Na<sub>2</sub>SO<sub>4</sub>), as would be expected based on solubility trends of iron. It should be noted that salt-bridges are thought to stabilize the tetrameric structure of E $\gamma$ CG. High concentrations of salt can disrupt these stabilizing, ionic interactions, leading to the hydrolysis of the iron-sulfur cluster.<sup>[13]</sup>

We also assessed the impact of chemical additives on iron-sulfur clusters coordinated to NAc-Cys-OMe, which had a much greater propensity to form [4Fe–4S] rather than [2Fe–2S] clusters (Figure 4, S13, Table S11–S13). The impact of many of the chemical additives, such as FeCO<sub>3</sub>, CaCO<sub>3</sub>, BH<sub>3</sub>O<sub>3</sub>, P<sub>4</sub>O<sub>10</sub>, and Na<sub>3</sub>P<sub>3</sub>O<sub>9</sub>, were similar to those observed with iron-sulfur E $\gamma$ CG. However, some differences were apparent. For example, diethyl phosphoramidate did not degrade the iron-sulfur cluster of NAc-Cys-OMe, whereas the same molecule disrupted the polynuclear iron-sulfur clusters of E $\gamma$ CG. Na<sub>2</sub>SiO<sub>3</sub> also appeared to be less disruptive for iron-sulfur clusters coordinated to NAc-

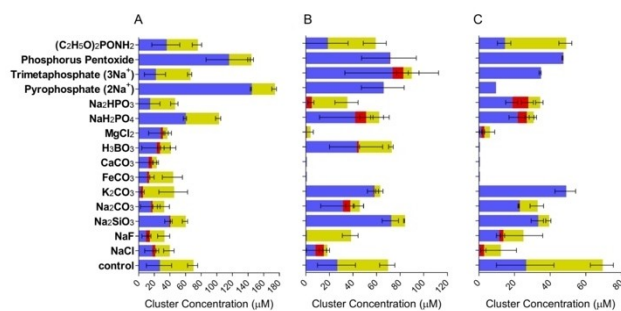


**Figure 4.** Iron-sulfur cluster composition of N-acetyl-L-cysteine methyl ester in the presence of different chemical additives at pH 8.7 and 100  $\mu\text{M}$  (A), 500  $\mu\text{M}$  (B), and 500 mM (C) chemical additive. Mononuclear centre is shown in blue, [2Fe–2S] in red, and [4Fe–4S] in yellow. Data represent mean and SD of distinct samples,  $n = 3$ .

Cys-OMe in comparison to E $\gamma$ CG. Conversely, iron-sulfur NAC-Cys-OMe was more sensitive to the presence of phosphite (added as  $\text{Na}_2\text{HPO}_3$ ), phosphate (added as  $\text{NaH}_2\text{PO}_4$ ),  $\text{Mg}^{2+}$  ( $\text{MgCl}_2$ ), and carbonate ( $\text{K}_2\text{CO}_3$  and  $\text{Na}_2\text{CO}_3$ ) than iron-sulfur E $\gamma$ CG. In the absence of structural information, it is difficult to determine the cause for these differences in stability. However, NAC-Cys-OMe is incapable of forming inter-molecular salt-bridges when coordinated to an iron-sulfur cluster, and thus would be expected to form less stable complexes. Although individual additives have definable effects on stability, the data alone cannot predict behavior in a complex environment. This is likely because different molecular components can interact in ways that either enhance or diminish the impact on the iron-sulfur cluster. We previously observed a similar situation with lipid membranes where the presence of  $\text{Na}^+$  protected against the degradative effects of  $\text{Mg}^{2+}$ .<sup>[14]</sup>

### Heat and Low pH Decrease Stability

To better define the range of conditions compatible with iron-sulfur clusters, we next assessed the impact of temperature and pH on iron-sulfur clusters coordinated to E $\gamma$ CG. Thermal stability was probed by placing iron-sulfur E $\gamma$ CG at different temperatures and monitoring degradation by absorbance at 420 nm (Figure S15–S20). Higher temperatures led to decreased half-lives (Figure 5A), with the half-life dropping 1.9-fold when the

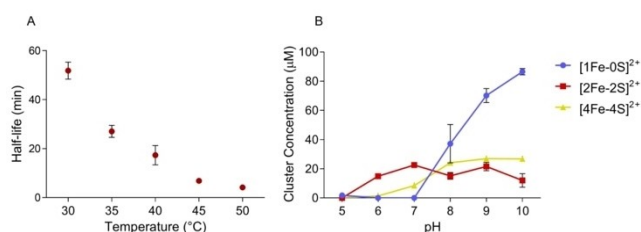


**Figure 5.** Thermal (A) and pH (B) stability. A. Half-lives of [2Fe–2S] cluster coordinated by E $\gamma$ CG. B. Iron-sulfur composition of samples at different pH after incubation for 2 h. Data obtained represent mean and SD of distinct samples,  $n = 3$ .

temperature was increased from 30  $^{\circ}\text{C}$  to 35  $^{\circ}\text{C}$ . To evaluate stability to pH, we attempted to synthesize iron-sulfur clusters at different pH and then assessed the iron-sulfur composition of the solution by UV-Vis spectral decomposition (Figure S21). The [4Fe–4S] cluster was more stable between pH 8 and 10 (Figure 5B). Low pH led to the degradation of iron-sulfur clusters, either through the protonation of thiolates or of bridging inorganic sulfides.<sup>[15]</sup> [2Fe–2S] clusters showed less of a dependence on pH, with data collected between pH 6 and 10 yielding similar amounts of [2Fe–2S] cluster. The data also indicated that the pH strongly impacted the type of iron-sulfur cluster formed at the tested environmental conditions. For example, mononuclear centers were favored at high pH and were observed to predominate under Alkaline Lake (pH 10) conditions. Nevertheless, the impact of the chemical composition of the solution was evident for Lost City conditions (pH 9), which favored the formation of [4Fe–4S] E $\gamma$ CG. Similarly, low pH favored the formation of [2Fe–2S] E $\gamma$ CG, consistent with the data collected at glacial brine (pH 5) conditions. However, seawater conditions (pH 6.5) lead to the formation of mostly mononuclear center. Destabilization of [2Fe–2S] E $\gamma$ CG at pH 6.5 may have been due to the presence of  $\text{Na}_2\text{SiO}_3$ .

### Conclusions

Iron-sulfur clusters ligated by small organic thiolates in aqueous solution exist in equilibrium between different structures.<sup>[16]</sup> It is, therefore, unsurprising to find that many factors exist that can disrupt this equilibrium and thus the type of iron-sulfur cluster formed. Our results reveal strong sensitivity of iron-sulfur clusters to high concentrations of chemical species that are intrinsic to a number of recently proposed prebiotic chemical systems, e.g., sulfite,<sup>[17]</sup> phosphate as a reactant, buffer, and catalyst<sup>[18]</sup> or as a phosphorylating agent,<sup>[19–21]</sup> and silicic acid.<sup>[22]</sup> As such, our results paint a general picture where model prebiotic iron-sulfur clusters are quite unstable in highly concentrated prebiotic subaerial basins. This result can be interpreted as evidence that a) the origins of life did not take place in such a setting; b) occurred in an unexpectedly silicate-, sulfite-, phosphate-poor variant of such an environment; or c) that iron-sulfur clusters arrived later either after prebiotic chemistry itself depleted these chemical disruptors in the local environment or after the emergence of more complex peptidyl scaffolds that could have better protected the iron-sulfur cluster from the environment.

As emphasis is often placed on exploiting a few simple, prebiotically plausible components rather than running reactions in more complex, environmentally reasonable conditions, it can be difficult to assess the likelihood of the observed chemistry. While it remains difficult to understand which conditions represent actual prebiotic environments, our data demonstrate that one cannot easily extrapolate from standard laboratory conditions to reactions in geologically realistic and therefore prebiotically plausible settings. Nevertheless, iron-sulfur clusters form over a wide variety of conditions, suggesting that such structures existed in the past. In the future, it will

be important to evaluate the likelihood of stabilizers or regenerative systems that could have facilitated the engagement of iron-sulfur clusters in chemistry useful to a protocell.

## Experimental Section

All reagents were obtained from Sigma Aldrich or BOC science and used without any further purification. Schlenk lines and Schlenk glassware were used throughout. Stock solutions were prepared with deoxygenated water that was made by distilling deionized ultrapure water (Synergy UV Water Purification System) under a flow of N<sub>2</sub>.

**Synthesis of iron-sulfur clusters.** Peptide solutions were prepared by mixing NAc-Cys-OMe or E<sub>7</sub>CG with FeCl<sub>3</sub> and Na<sub>2</sub>S in a glass vial under anaerobic conditions using nitrogen distilled water. Subsequently, the pH was adjusted. Iron-sulfur glutathione (40 mM) was synthesized with 0.185 mM Na<sub>2</sub>S, 0.5 mM FeCl<sub>3</sub>, pH 8.7. Iron-sulfur NAc-Cys-OMe (5 mM) was synthesized with 0.8 mM Na<sub>2</sub>S, 0.4 mM FeCl<sub>3</sub>, pH 8.7.

**UV-vis spectroscopy.** UV-vis absorption spectra were collected with an Agilent Cary 3500 UV-Vis spectrometer with 0.02 s integration and an interval of 1 nm. Samples were prepared under anaerobic condition and transferred to sealed quartz cuvettes (path length = 1 cm).

**Data Analysis.** UV-vis spectra were fit with Fit-FeS.<sup>[11]</sup> Reference spectra for the mononuclear center and the [2Fe–2S] and [4Fe–4S] clusters were collected with organic thiolate:Fe<sup>3+</sup>:HS<sup>-</sup> of 4:1:0, 4:1:1, and 4:1:2, respectively.

**Mössbauer Spectroscopy.** Samples were prepared with <sup>57</sup>FeCl<sub>3</sub> in place of regular FeCl<sub>3</sub>. After the iron-sulfur cluster was synthesized, the complex was precipitated by using 40X volume of degassed isopropanol or ethanol. The solution was centrifuged at 12,000 rpm for 30 min at 4 °C with an Avanti J-26S XP centrifuge. The solvent was discarded, and the iron-sulfur cluster pellet was left to dry under a flux of nitrogen overnight. Mössbauer measurements were acquired at 80 K with a standard setup in transmission geometry comprising a Kr-CO<sub>2</sub> proportional counter, FastTM electronics for gamma ray spectroscopy, and a WisselTM spectrometer, which was run in sinusoidal acceleration mode ( $v_{\max} = 5.0$  mm/s) and calibrated by using a standard metal iron foil. The  $\gamma$ -ray source was a 7-mCi <sup>57</sup>Co in rhodium matrix with Lamb-Mössbauer factor  $f = 0.63$ , measured as previously described.<sup>[23]</sup> For the measurement at 80 K, a N<sub>2</sub>-based Oxford flux cryogenic system was used. Approximately 46 mg/cm<sup>2</sup> of each compound were used for the measurements. Mössbauer spectra were interpreted by means of a fitting procedure based on the evaluation of the transmission integral function that takes into account the dependence of the Mössbauer spectra on the sample effective thickness. The complete expression used to fit the spectra was:  $Y(v) = N_b(v) \left\{ 1 - f_s^r \int_{-\infty}^{\infty} L_s(\omega - v, \Gamma_s) \left[ 1 - e^{-t_a \sigma(\omega)} \right] d\omega \right\}$ , where  $Y(v)$  and  $N_b(v)$  are the detected counts and the spectrum baseline, respectively, as a function of the transducer velocity  $v$ .<sup>[24]</sup> Moreover,  $f_s^r$  is the reduced recoilless fraction of the source and  $L_s(\omega - v, \Gamma_s)$  is the Voigt distribution (having  $v$  and  $\Gamma_s$  as center and FWHM, respectively) used to describe the source

line shape. The Voigt profile has a Lorentzian component with natural linewidth, while that of the Gaussian one is suitable to reproduce the total linewidth of the source provided by the manufacturer ( $\Gamma_s = 0.114$  mm/s). Finally,  $\sigma(\omega)$  is the absorption cross-section of the sample as a function of the energy  $\omega$ , expressed in mm/s, and  $t_a$  is the effective thickness of the sample. In the limit of 'thin absorption approximation' ( $t_a < 1$ ), each contribution to  $\sigma(\omega)$  is expressed as a Voigt doublet having a Lorentzian component with the natural linewidth ( $\Gamma_n$ ) and a Gaussian one with broadening  $\sigma$ , describing a distribution of hyperfine parameters.<sup>[25]</sup> Consequently, the total linewidth of each contribution is approximately given by  $\Gamma_{\text{tot}} = \Gamma_s + \Gamma_n + \sigma$ . Multiple contributions characterized by different values of the hyperfine parameters were used to fit the spectra and were assigned to the iron-sulfur clusters by comparison with data reported in literature.<sup>[26,27]</sup> For all samples a rather good agreement between experimental and best fit data was obtained with  $\chi^2 \sim 1000$  for the 512 points.

## Acknowledgments

We acknowledge support from the Simons Foundation (290358FY19) and the Natural Sciences and Engineering Research Council of Canada (NSERC) [RGPIN-2020-04375].

## Conflict of Interests

The authors declare no conflict of interest.

## Data Availability Statement

The data that support the findings of this study are available in the supplementary material of this article.

**Keywords:** Iron-sulfur cluster · Metallopeptide · Prebiotic chemistry · Bioinorganic chemistry · Prebiotic environments

- [1] H. Beinert, *JBC J. Biol. Inorg. Chem.* **2000**, *5*, 2–15.
- [2] W. Qi, J. Li, C. Y. Chain, G. A. Pasquevich, A. F. Pasquevich, J. A. Cowan, *J. Am. Chem. Soc.* **2012**, *134*, 10745–10748.
- [3] C. Bonfio, L. Valer, S. Scintilla, S. Shah, D. J. Evans, L. Jin, J. W. Szostak, D. D. Sasselov, J. D. Sutherland, S. S. Mansy, *Nat. Chem.* **2017**, *9*, 1229–1234.
- [4] S. Scintilla, C. Bonfio, L. Belmonte, M. Forlin, D. Rossetto, J. Li, J. A. Cowan, A. Galliani, F. Arnesano, M. Assfalg, S. S. Mansy, *Chem. Commun.* **2016**, *52*, 13456–13459.
- [5] J. D. Toner, D. C. Catling, *Proc. Natl. Acad. Sci. USA* **2020**, *117*, 883–888.
- [6] A. P. Webber, S. Roberts, B. J. Murton, M. R. S. Hodgkinson, *Geochim. Geophys. Geosystems Res.* **2015**, *16*, 2661–2678.
- [7] A. M. Colín-García, A. Heredia, G. Cordero, A. Camprubí, A. Negrón-Mendoza, F. Ortega-Gutiérrez, H. Beraldi, S. Ramos-Bernal, M. Colín-García, A. Heredia, G. Cordero, A. Camprubí, A. Negrón-Mendoza, F. Ortega-Gutiérrez, H. Beraldi, S. Ramos-Bernal, *Bol. Soc. Geol. Mex.* **2016**, *68*, 599–620.
- [8] C. Jones, S. Nomosatryo, S. A. Crowe, C. J. Bjerrum, D. E. Canfield, *Geology* **2015**, *43*, 135–138.

- [9] W. B. Lyons, J. A. Mikucki, L. A. German, K. A. Welch, S. A. Welch, C. B. Gardner, S. M. Tulaczyk, E. C. Pettit, J. Kowalski, B. Dachwald, *J. Geophys. Res. [Biogeosci.]* **2019**, *124*, 633–648.
- [10] C. R. Walton, P. Rimmer, O. Shorttle, *Front. Earth Sci.* **2022**, *10*, 1–12.
- [11] I. O. Betinol, S. Nader, S. S. Mansy, *Anal. Biochem.* **2021**, *629*, 114269.
- [12] P. Venkateswara Rao, R. H. Holm, *Chem. Rev.* **2004**, *104*, 527–559.
- [13] J. Li, S. A. Pearson, K. D. Fenk, J. A. Cowan, *J. Biol. Inorg. Chem.* **2015**, *20*, 1221–1227.
- [14] D. Toparlak, M. Karki, V. Egas Ortuno, R. Krishnamurthy, S. S. Mansy, *Small* **2020**, *16*, 1–8.
- [15] S. S. Mansy, Y. Xiong, C. Hemann, R. Hille, M. Sundaralingam, J. A. Cowan, *Biochemistry* **2002**, *41*, 1195–1201.
- [16] L. Valer, D. Rossetto, S. Scintilla, Y. J. Hu, A. Tomar, S. Nader, I. O. Betinol, S. Mansy, *Can. J. Chem.* **2022**. DOI: 10.1139/cjc-2021-0237.
- [17] J. Xu, D. J. Ritson, S. Ranjan, Z. R. Todd, D. D. Sassellov, J. D. Sutherland, *Chem. Commun.* **2018**, *54*, 5566–5569.
- [18] B. H. Patel, C. Percivalle, D. J. Ritson, C. D. Duffy, J. D. Sutherland, *Nat. Chem.* **2015**, *7*, 301–307.
- [19] M. A. Pasek, *Chem. Rev.* **2020**, *120*, 4690–4706.
- [20] D. Gan, J. Ying, Y. Zhao, *Front. Chem.* **2022**, *10*, 1–10.
- [21] A. W. Schwartz, *Philos. Trans. R. Soc. B Biol. Sci.* **2006**, *361*, 1743–1749.
- [22] R. Siever, *Geochim. C* **1992**, *56*, 3265–3272.
- [23] G. Spina, M. Lantieri, *Nucl. Instrum. Methods Phys. Res. Sect. B* **2014**, *318*, 253–257.
- [24] Y. Chen, D. Yang, *Mössbauer Eff. Lattice Dyn.* **2007**. DOI: 10.1002/9783527611423.
- [25] M. Bini, S. Ferrari, D. Capsoni, P. Mustarelli, G. Spina, F. Del Giallo, M. Lantieri, C. Leonelli, A. Rizzuti, V. Massarotti, *RSC Adv.* **2012**, *2*, 250–258.
- [26] M.-E. Pandelia, N. D. Lanz, S. J. Booker, C. Krebs, *Biochim. Biophys. Acta Mol. Cell Res.* **2015**, *1853*, 1395–1405.
- [27] C. Ueda, M. Langton, M.-E. Pandelia, *Fe–S Proteins Methods Protoc.* **2021**, *2353*, 281–305.

---

Manuscript received: June 28, 2024

Accepted manuscript online: September 18, 2024

Version of record online: ■■, ■■